UNIVERSITY OF COPENHAGEN



Københavns Universitet

Adaptive polymer fiber neural device for drug delivery and enlarged illumination angle for neuromodulation

Sui, Kunyang; Meneghetti, Marcello; Daniil, Jaspreet Kaur; Sørensen, Roar Jakob Fleng ; Berg, Rune W.; Markos, Christos

Published in:
Journal of Neural Engineering

DOI:
10.1088/1741-2552/ac5267

Publication date:
2022

Document version
Peer reviewed version

Document license:
CC BY-NC-ND

Citation for published version (APA):
Sui, K., Meneghetti, M., Daniil, J. K., Sørensen, R. J. F., Berg, R. W., & Markos, C. (2022). Adaptive polymer fiber neural device for drug delivery and enlarged illumination angle for neuromodulation. *Journal of Neural Engineering*, *19*(1), Article 016035. https://doi.org/10.1088/1741-2552/ac5267

Download date: 13. Nov. 2026

Journal of Neural Engineering

ACCEPTED MANUSCRIPT

Adaptive polymer fiber neural device for drug delivery and enlarged illumination angle for neuromodulation

To cite this article before publication: Kunyang Sui *et al* 2022 *J. Neural Eng.* in press https://doi.org/10.1088/1741-2552/ac5267

Manuscript version: Accepted Manuscript

Accepted Manuscript is "the version of the article accepted for publication including all changes made as a result of the peer review process, and which may also include the addition to the article by IOP Publishing of a header, an article ID, a cover sheet and/or an 'Accepted Manuscript' watermark, but excluding any other editing, typesetting or other changes made by IOP Publishing and/or its licensors"

This Accepted Manuscript is **© 2022 IOP Publishing Ltd**.

During the embargo period (the 12 month period from the publication of the Version of Record of this article), the Accepted Manuscript is fully protected by copyright and cannot be reused or reposted elsewhere.
As the Version of Record of this article is going to be / has been published on a subscription basis, this Accepted Manuscript is available for reuse under a CC BY-NC-ND 3.0 licence after the 12 month embargo period.

After the embargo period, everyone is permitted to use copy and redistribute this article for non-commercial purposes only, provided that they adhere to all the terms of the licence https://creativecommons.org/licences/by-nc-nd/3.0

Although reasonable endeavours have been taken to obtain all necessary permissions from third parties to include their copyrighted content within this article, their full citation and copyright line may not be present in this Accepted Manuscript version. Before using any content from this article, please refer to the Version of Record on IOPscience once published for full citation and copyright details, as permissions will likely be required. All third party content is fully copyright protected, unless specifically stated otherwise in the figure caption in the Version of Record.

View the article online for updates and enhancements.

This content was downloaded from IP address 192.38.90.17 on 15/02/2022 at 14:58

IOP Publishing Journal Title
Journal **XX** (XXXX) XXXXXX https://doi.org/XXXX/XXXX

Adaptive polymer fiber neural device for drug delivery and enlarged illumination angle for neuromodulation

Kunyang Sui[1,2], Marcello Meneghetti[1], Jaspreet Kaur[2], Jakob Fleng Sørensen[2], Rune W. Berg[2] and Christos Markos[1]

[1] DTU Fotonik, Technical University of Denmark, Lyngby, Denmark
[2] Department of Neuroscience, Faculty of Health and Medical Sciences, University of Copenhagen, Copenhagen, Denmark

E-mail: chmar@fotonik.dtu.dk

Received xxxxxx
Accepted for publication xxxxxx
Published xxxxxx

Abstract

Objective. Optical fiber devices constitute significant tools for the modulation and interrogation of neuronal circuitry in the mid and deep brain regions. The illuminated brain area during neuromodulation has a direct impact on the spatio-temporal properties of the brain activity and depends solely on the material and geometrical characteristics of the optical fibers. In the present work, we developed two different flexible polymer optical fibers (POFs) with integrated microfluidic channels (MFCs) and an ultra-high numerical aperture (UHNA) for enlarging the illumination angle to achieve efficient neuromodulation. *Approach*. Three distinct thermoplastic polymers: polysulfone (PSU), polycarbonate (PC), and fluorinated ethylene propylene (FEP) were used to fabricate two step-index UHNA POF neural devices using a scalable thermal drawing process. The POFs were characterized in terms of their illumination map as well as their fluid delivery capability in phantom and adult rat brain slices. *Main results.* A 100-fold reduced bending stiffness of the proposed fiber devices compared to their commercially available counterparts has been found. The integrated MFCs can controllably deliver dye (trypan blue) on-demand over a wide range of injection rates spanning from 10 nL/min to 1000 nL/min. Compared with commercial silica fibers, the proposed UHNA POFs exhibited an increased illumination area by 17% and 21% under 470 and 650 nm wavelength, respectively. In addition, a fluorescent light recording experiment has been conducted to demonstrate the ability of our UHNA POFs to be used as optical waveguides in fiber photometry. *Significance*. Our results overcome the current technological limitations of fiber implants that have limited illumination area and we suggest that soft neural fiber devices can be developed using different custom designs for illumination, collection, and photometry applications. We anticipate our work to pave the way towards the development of next-generation functional optical fibers for neuroscience.

Keywords: neural device, polymer optical fibers (POFs), flexible, microfluidic channels (MCs), ultra-high numerical aperture (UHNA), brain slices, neuromodulation

Accepted Manuscript

 © xxxx IOP Publishing Ltd

1. Introduction

Neuromodulation is a broadly used method in neuroscience that relies on an external stimulus (e.g. electrical signals or chemical agents) delivered to a target site for modulating neuronal activities [1]. However, traditional neuromodulation methods can hardly achieve spatio-temporal access to the target neural population at a single neuron resolution [2]. Electrical stimulation, for instance, despite its high temporal precision, indiscriminately targets all cells in a large volume, resulting in a significant limitation in terms of specificity. Optogenetics, on the other hand, is a powerful biological technique that enables light-based modulation of genetically modified neurons with a millisecond time resolution and high cell-type specificity [3]. This powerful technique has been widely used to study the functional connectivity of neural circuits in the past two decades [4]. Although light-based techniques can directly affect the neuronal response in a non-invasive way [5], the quick attenuation of the light propagating in the tissue due to the combined effect of absorption and scattering makes this approach impractical for deep-tissue optical neuromodulation [6].

Implantable optical fibers have been considered as very effective tools to overcome this limitation [7–9]. Since the first demonstration of *in vivo* optogenetic neuromodulation in rodents based on silica fibers [7], silica has become the most commonly used material for fiber-based neuromodulation. This is due to its high stability, low loss in the wavelength range from visible to near-infrared, and commercial availability. However, the fragile and brittle nature of silica glass makes it easy to get fractured, resulting in shards and jagged edges likely to cause tissue damage [8]. In addition, the bending stiffness of silica fibers is several orders of magnitude higher than the one of organic tissue, leading to undesirable inflammatory responses when they are used as an optogenetic device for long-term chronic implants [10]. Moreover, the difference in the refractive index (RI) of the core and cladding is strongly limited by the standard production technique for silica step-index fibers, which relies on the use of dopants. Indeed, the amount of dopant in the core needed to obtain a large RI core-cladding contrast would lead to a significant change in the material's thermal expansion coefficient. This could subsequently increase residual thermal stresses and cause the fracture of the fibers in the drawing process [11]. As a result, silica optical fibers with a numerical aperture (NA) larger than 0.5 are not readily available [12].

The aforementioned mechanical mismatch between the optical waveguide and the tissue can be mitigated by the use of polymer optical fibers (POFs). POFs have attracted significant attention since the late 1960s [13]. Over the following decades, POFs have developed into a versatile platform, mainly for a range of sensing applications [14–16]. With the recent fast development of optogenetics, POFs have been employed as an emerging implantable platform for neuronal excitation and recording. SU8 [17], poly(ethylene glycol) (PEG) [18], poly(L-lactic acid) (PLA), and general poly lactic-co-glycolic acid (PLGA)-based polymers [19] have been used as optical waveguides for biomedical applications. However, the devices mentioned above are based on the use of a single core material without a cladding structure, leading to high optical losses and high sensitivity to external perturbations since the light that propagates in the fiber interacts with the surrounding medium. In order to avoid the influence of the external environment, step-index fibers using for example polycarbonate (PC) as core and cyclic olefin copolymer (COC) as cladding material have been employed for optogenetic applications [20–23]. Interestingly, Canales *et al.* proposed a multifunctional fiber with a step-index PC/COC structure for simultaneous optical, electrical and chemical interrogation of neural circuits *in vivo* [21] while Frank *et al.* demonstrated a similar fiber device with the same optical waveguide structure for *in vivo* photopharmacology [22]. A biodegradable step-index optical fiber that is based on poly(octamethylene citrate) (POC) and poly(octamethylene maleate citrate) (POMC) was proposed by Shan *et al.* for *in vivo* deep tissue light delivery and fluorescence sensing experiment in rats [24]. Recently, Guo *et al.* demonstrated a fiber bundle with 4 BiSn electrodes and 60 optical fiber pixels whose core and cladding are made of PC and poly(methyl methacrylate) (PMMA) for recording local field potentials in the hippocampus of a mouse [25]. Although the reported POFs have achieved good performance for neuromodulation applications, the low RI difference between the core and cladding materials leads to a very low NA, which ultimately limits the illumination angle during optical neuromodulation [26].

This work reports for the first time the fabrication and characterization of two UHNA POFs. These results were obtained by employing fluorinated ethylene propylene (FEP) polymer, which has an extremely low RI, as cladding for the step-index structure of the two POFs. Their unique mechanical properties were evaluated by numerical analysis towards their use in long-term chronic implantation in the brain. MFCs were added to the cladding of one of the presented POFs to demonstrate their potential to be used as multifunctional neural devices. The illumination properties of the fibers were also characterized and compared to commercially available silica fibers using both artificial (phantom) and adult rat brain slices. Finally, a fiber photometry experiment was conducted in order to verify the ability of our fibers to collect fluorescent light from the tissue. The enlarged illumination angle given by their UHNA (>0.8), combined with the high flexibility and the MFCs, makes the presented neural devices valuable tools in optical neuromodulation for simultaneous on-demand drug delivery, enlarged illumination angle, and fluorescence light collection.

Accepted Manuscript

2. Materials and methods

2.1 Material properties

To produce high-quality UHNA polymer step-index fibers by thermal drawing, the core and cladding materials should be thermally compatible while having a large difference in RI. The polymers used for the fabrication of the POFs were: PC/FEP and PSU/FEP. PSU and PC were the core materials for the two fibers, and FEP was the cladding material for both of them. PSU is an amorphous, high-strength thermoplastic with a very high RI in the whole visible wavelength range. PC is a very commonly used waveguide material in optogenetics and sensing applications because of its high transparency in the visible and near-infrared region [27]. FEP is a copolymer of hexafluoropropylene and tetrafluoroethylene. It is an ideal cladding material for both PC and PSU core fibers due to: firstly, FEP is very soft (Young's modulus of FEP is 0.48 GPa [28], compared to that of silica is 70 GPa [29]), and therefore can highly increase the overall flexibility of the optical waveguide, a crucial property to achieve long-term deep tissue neuromodulation and minimize the foreign body response (FBR) [30]. Secondly, FEP has one the lowest RI within all the thermoplastics (1.34@630 nm [31]). The large RI difference between the core materials (PC, PSU) and the cladding material FEP leads to the UHNA of the POFs.

The RIs of the bulk PSU, PC, and FEP materials were measured using an ellipsometer (J.A.Woollam, VASE), which covers a broad wavelength range of 210-1690 nm with a 5-nm resolution for the range 210-1000 nm. The results are shown in figure 1(a). The NA of the fibers was calculated from the measured values of RI as [32]:

$$NA = \sqrt{n_{core}^2 - n_{cladding}^2}$$

where n_{core} corresponds to the RI of the core and $n_{cladding}$ to the RI of the cladding. The NA of PC/FEP and PSU/FEP POFs at different wavelengths are also depicted in figure 1(a) for reference.

As shown in figure 1(a), the NA difference between the PC/FEP and PSU/FEP POFs at wavelengths shorter than 500 nm is very small. However, at longer wavelengths (>600 nm) the NA profile of PC/FEP POFs exhibits a significant reduction compared to PSU/FEP POFs due to their different material dispersion.

The main requirement for materials to be thermally compatible in terms of fiber fabrication is that they must have a relatively close softening temperature. Viscosity as a function of temperature is the main parameter that defines the thermal compatibility between materials [33]. In figure 1(b), the viscosity-temperature curves of PSU and FEP were measured using a rotational rheometer (TA, Discovery Hybrid HR-2). The measurement shows that the viscosity of PSU is relatively high at low temperatures and as the temperature increases it starts expanding and changing from a solid to a rubbery state. In this case, the viscosity decreases significantly and reaches a relatively rubbery plateau region as temperature further increases. For FEP, the viscosity at first decreases slowly with the increase of temperatures, and above ~260°C, the decrease is prone to be dramatic since the material became less viscous. By contrast, the viscosity of PC simply decreases with the increase of temperature [34].

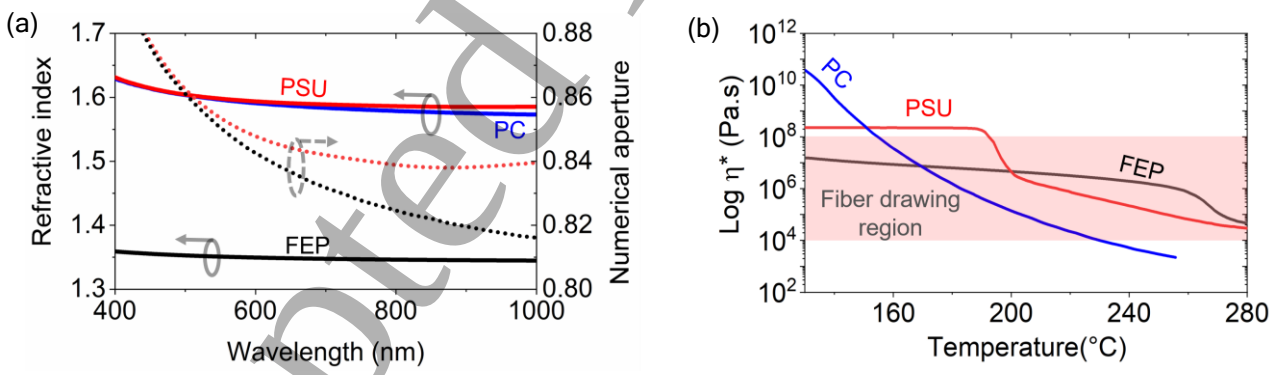


Figure 1. (a) RI of PSU (red solid line), PC (blue solid line), and FEP (black solid line) as a function of wavelength, and the calculated NA for PSU/FEP POFs (red dot line), PC/FEP POFs (black dot line). (b) Viscosity as a function of the temperature of PC (blue solid line – extracted from Ref. [34]), PSU (red solid line), and FEP (black solid line). The target viscosity region for fiber drawing is highlighted in the red area.

2.2 Fiber fabrication

The fiber preforms were assembled by the rod-in-tube method, starting with a PC and PSU rod of 10 mm diameter and they were inserted into two pre-machined FEP tubes (inner diameter: 10.5 mm; Outer diameter: 25.5 mm), respectively as depicted in figure 2(a). As an added functionality in the PC/FEP POFs, two hollow channels with

Accepted Manuscript

an initial diameter of 4 mm were drilled in the FEP tube acting as the final MFCs. The two preforms, having a length of 10 cm, were then drawn into 100's of meters of fibers using a thermal drawing method in an optical fiber draw tower equipped with a 3-zone furnace (figure 2(b)). During the drawing process, the viscosity must be held relatively low, typically in the range from 10^4 to 10^8 Pa.s [35]. From figure 1(b), it can be seen that the PSU/FEP preform should be drawn at temperatures between ~200°C and ~280°C. By contrast, the PC/FEP preform should be drawn at lower temperatures spanning from ~160°C to ~230°C. During the drawing process, the diameter of the optical fiber was monitored by a laser diameter gauge with < 0.1 µm resolution. The fiber was continuously pulled at a fixed 0.2 mm/min feeding speed, while the drawing speed was adjusted accordingly during the process until the desired fiber diameter was achieved. The total diameter of the fabricated fiber ranges from 350 µm to 500 µm in order to be compatible with commercial connectorization components for implantation (cannula, ferrules, etc.). The drawn UHNA POFs were mechanically cleaved using a razor blade and inspected in an optical microscope to observe the cross-section interface. Figures 2(c) and 2(d) show the optical microscope images of the PC/FEP POFs with a core/cladding diameter of 200/420 µm and PSU/FEP POFs with a core/cladding diameter of 185/450 µm, respectively. Since our main goal is only to demonstrate the adaptability of the proposed fibers towards multifunctionalization, here we only introduced two MFCs into the PC/FEP fibers. However, it should be noted that more MFCs or metal electrodes can be added to the fibers if one wants to reach faster drug injection speeds or record neural electrical activity, respectively [21,22]. This feature can also be replicated in the PSU/FEP fibers.

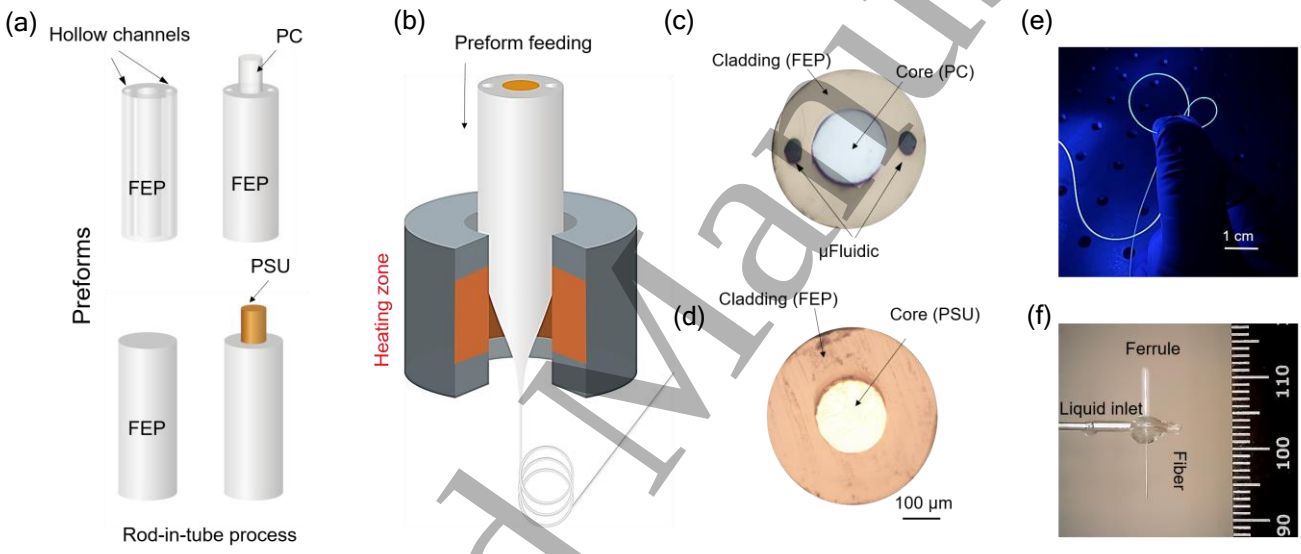


Figure 2. (a) Schematics of the rod-in-tube method for making the preforms. For the preform of PC/FEP POFs, two additional holes were drilled in the FEP tube in order to introduce MFCs in the corresponding fiber. (b) Schematics of the thermal drawing method employed to fabricate the presented POFs. (c),(d) Optical microscope images of the drawn step-index PC/FEP POFs and PSU/FEP POFs, respectively. (e) Blue light propagates in the PC/FEP POFs after being bent with a sub-centimeter radius. (f) An assembled neural device with both the waveguide and the MFCs connectorized.

2.3 Mechanical flexibility modeling and MFCs characterization

When conventional neural devices are implanted in the tissue for long-term neuromodulation, the mechanical mismatch between the devices and the brain tissue leads to neuronal death and inflammatory response [36]. This FBR can be mitigated by using more flexible neural devices [37]. Bending stiffness is thus a general parameter that defines the overall mechanical flexibility of the implants. Assuming the case of the device being fixed to the skull or vertebrae, bending stiffness is defined as the force (F) required to reach a certain deflection (d) [38]:

$$\frac{F}{d} = \frac{48EI}{L^3}$$

where E is the composite Young's modulus of the different materials calculated from the device's geometry, I is the moment of inertia, and L is the length of the neural probe.

Accepted Manuscript

The fabricated POFs were found to be very flexible and can be easily bent at small radii as illustrated in figure 2(e). To quantitatively evaluate the flexibility of the structured POFs, a numerical analysis based on COMSOL Multiphysics was used to simulate the bending condition and calculate the corresponding bending stiffness. A 3D finite-element model of the probe was developed and the ratio between the core and cladding diameter of the UHNA POFs was set to 2:5, the same as the one of the initial preforms. One end of the fiber was fixed and a force perpendicular to the axial direction was applied to the other end. We compared the bending stiffness of the fabricated UHNA POFs with three other optical waveguides: silica fibers, the most commonly used optical waveguide in optogenetics; fluoropolymer (CYTOP) fiber, a kind of commercially available POF which has significantly low optical loss; PMMA fibers, another conventional and widespread type of POF in optogenetics [39]. To evaluate the geometrical/size impact of the mechanical flexibility, we calculated the bending stiffness of the fabricated UHNA POFs with diameters ranging from 100 to 500 μm and lengths ranging from 8 to 13 mm. The Young's moduli of the five materials used in our simulations were retrieved from the literature and are shown in Table 1.

Table 1. The Young's Modulus Used in Numerical Analysis

Materials [Ref.]	PMMA [40]	PSU [41]	FEP [28]	Silica [29]	CYTOP [42]
Young's Modulus (GPa)	3	2.48	0.48	70	1.6

To test the drug delivery ability of the PC/FEP fiber, the MFCs were carefully exposed from the side of the fiber with a scalpel under a microscope (Zeiss, Axioscope) and connected with a syringe using a low-density polyethylene tube (Goodfellow, ET317150, inner diameter: 0.9 mm, outer diameter: 1.1 mm). The gap between the fiber and the tube was sealed using an epoxy resin (Thorlabs, G14250). The fully assembled device is shown in figure 2(f). The probe was inserted into the prepared brain phantom and the injection was driven by an electrical syringe pump (Harvard, PHD 2000). To demonstrate the stable fluid delivery using the MFCs of the implanted PSU/FEP probe, we injected 10 μL trypan blue staining dye (Sigma-Aldrich, T8154) with a target rate of 10, 50,100, 500, and 1000 nL/min, respectively. The output rate was calculated by dividing the output volume by the time required for achieving the injection.

2.4 Brain phantom, ethical approval, and brain slice preparation

The illumination maps of the optical fibers were firstly measured in a brain phantom (0.6% agarose) as the propagation medium. It has been extensively demonstrated that 0.6% agarose gels can be used as a surrogate material as a brain tissue model towards diagnostic and therapeutic applications [43]. To prepare the brain phantom, agarose gels were dissolved in distilled water with a concentration of 0.6% (wt/vol). The solution was heated using a microwave oven and poured into a petri dish. After the solidification at room temperature, the phantom was sectioned using a vibratome into 20 x 20 x 1 mm slices.

In order to investigate the performance of our fiber devices in real brain tissue, wild-type adult rats were employed afterward as a more realistic model for the actual propagation of light during *in vitro* experiments. The procedure to prepare the fixed brain slices presented below is approved by the Animal Experiments Inspectorate under the Danish Ministry of Food, Agriculture, and Fisheries, and all procedures adhere to the European guidelines for the care and use of laboratory animals, EU directive 2010/63/EU. A Long-Evans wild-type adult rat was anesthetized by intraperitoneal injection of 200 mg/kg sodium pentobarbital. Hereafter, the level of anesthesia was assessed by pedal reflex pain response to firm toe pinch. Once a sufficient level of anesthesia was reached, the chest cavity was opened to expose the heart. A catheter, connected to a peristaltic pump (Gilsion, minipuls3), was inserted into the left ventricle of the heart, and a small incision was made into the vena cava inferior for perfusion. The perfusion of the rat was performed with 30 ml of 1X phosphate-buffered saline (BPS) followed by 30 ml of 4% paraformaldehyde (PFA) at the rate of 7.8 ml/min [44]. The rat was subsequently decapitated using a guillotine. The brain was dissected out and directly put into ice-cold 4% PFA. After fixation for 4 hours at 4°C, the brain was transferred to 30% sucrose (w/v) for cryoprotection at 4°C[45–47]. The whole rat brain and the cross-section used in the experiments are shown in figure 3. A vibratome (LEICA, VT1200) was then used to section the brain into slices. To facilitate sectioning, the brain was embedded in 3% agarose gels prepared with a method similar to the one for preparing the 0.6% gels described above. The slicing was conducted in ice-cold 1X PBS. Two different brain slice thicknesses were prepared: 700 μm for measuring the illumination map and 100 μm for the fluorescent light collection experiment described in section 3.4.

2.5 Illumination map characterization

As shown in figure 1(a), the PC/FEP POFs have a high NA for wavelengths shorter than 550 nm. Therefore, they are ideal for neuromodulation based on the activation of standard channelrhodopsins (ChRs), which have absorption peaks in the 450–545 nm range [48,49]. Recently, red-shifted variants of ChRs have attracted significant attention since the tissue absorption and scattering is significantly reduced (6 times lower) for the red light, allowing deeper penetration into biological tissues compared to blue light [50–52]. The

Accepted Manuscript

PSU/FEP POFs are thus more efficient as optical waveguides for red-shifted ChRs because they offer higher NA than that of PC/FEP POFs at wavelengths longer than ~600 nm. Therefore, the illumination map of the PC/FEP POFs was measured with blue light (wavelength λ = 470 nm) and that of PSU/FEP POFs was measured with red light (λ = 650 nm). For both cases, the core diameter was chosen to be 200 µm in order to directly compare their illumination maps with that of the commercial silica fibers (Thorlabs, FT200EMT, core diameter: 200 µm, NA: 0.39), which are extensively used in optogenetics [53–55]. To measure the illumination map of PC/FEP POFs, a LED with a central wavelength at 470 nm (Thorlabs, M470L4) was used. The light was coupled to the fiber after being collimated with an aspheric lens (L1), passed through a bandpass filter (F1) with center wavelength at 470 nm (Thorlabs, FB470-10), and then reflected by a dielectric (Thorlabs, BB1-E02) and a dichroic mirror (Thorlabs, DMLP650R) as shown in figure 3. Similarly, for the PSU/FEP POFs, a LED with a central wavelength at 650 nm (Thorlabs, M650L4) was coupled to the fiber using the same method as mentioned before. We then evaluated the performance of every fiber by inserting them both in phantoms (0.6% agarose gels) and brain slices (configuration 1 in figure 3). The illumination maps were measured by recording the scattered light perpendicularly to the propagation direction using a digital microscope (Dino-Lite, AM7915MZT). This particular configuration was found to be an efficient way to characterize our fibers since the light-tissue interaction at visible wavelengths is strongly scattering-dominated [56]. For example, at 674 nm wavelength, the scattering coefficient of cortical human tissues is 124 cm^{-1}. By contrast, the absorption coefficient is only 0.17 cm^{-1} [57].

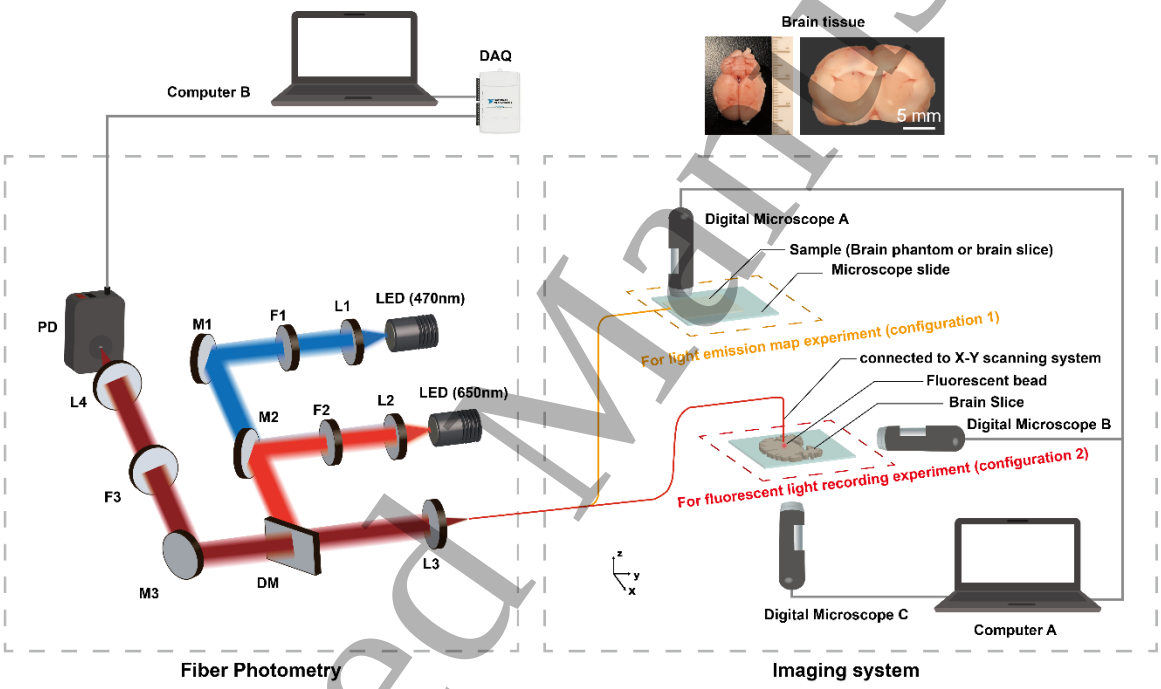


Figure 3. Schematic of the experimental setup for measuring the illumination map of UHNA PSU/FEP POFs, PC/FEP POFs, commercial silica fibers, and testing the viability of the UHNA POFs for fluorescent light recording in fiber photometry in the brain slice. (L1: Lens1. F1: Filter1. M1: Mirror1. L2: Lens2. F2: Filter2. M2: Mirror2. DM: Dichroic Mirror. L3: Lens3. M3: Mirror3. F3: Filter3. L4: Lens4. PD: Photodetector. DAQ: Data acquisition system).

2.6 Fiber photometry and fluorescent light recording

Fiber photometry is one of the fundamental methods for optical interrogation of neural circuits with cell specificity and high temporal and spatial resolution [58]. Since most of the techniques rely on the implantation of optical fibers in the brain, fiber photometry can eventually induce tissue damage due to FBR over chronic experiments [10]. Since a major advantage of the fabricated implantable fiber devices is their soft cladding material (FEP) that can mitigate the FBR, an *in vitro* fluorescent light recording experiment was conducted to show their ability to be used in fiber photometry. The experimental setup included two main parts: a custom-built

Accepted Manuscript

fiber photometry setup and an imaging system, as shown in figure 3 (configuration 2). A polystyrene (PS) microsphere with a diameter of 15 μm (Thermo Fisher Scientific, F8843) was embedded into a 100 μm thick brain slice and placed on a microscope slide to simulate the fluorescent signal emitted from an activated single neuron [59,60]. The excitation and emission peaks of the fluorescent PS beads have their maxima at 650 nm and 680 nm, respectively. An LED with a central wavelength at 650 nm was coupled to the fiber and was used as the excitation wavelength of the PS. The fluorescence signal from the PS bead was collected by the same optical fiber. The backward fluorescent light was reflected (M3) and filtered by a bandpass filter (F3) with a center wavelength at 680 nm (Thorlabs, FB680-10), and finally focused on a sensitive photodetector (Newfocus 2151, Newport) with a photosensitive area of 1x1 mm^2. In the imaging system, a motorized 2D scanning stage (Standa, 8MTF) was employed to mount the optical fiber and scan the position of the fiber in the X and Y direction. Two digital microscopes that connected to a computer were used to monitor the relative position between the optical fiber's tip and the sample. A DAQ (USB-6211) from National Instruments and a custom-made program in Labview software were used to scan and collect the emitted fluorescent signal from the photodetector.

3. Results

3.1 Mechanical flexibility and MFCs characterization

Figure 4(a) shows the numerical analysis of the bending stiffness for PSU/FEP, PC/FEP, silica, PMMA, and CYTOP optical fibers. For a direct comparison between the data, the diameter of the fibers was normalized to 400 μm as most multifunctional neural probes used by researchers have a diameter between 300 μm and 500 μm [21,22,61]. The bending stiffness of the PSU/FEP and PC/FEP fiber was found to be almost two orders of magnitude lower than the commonly used silica fibers. Due to the low Young's modulus of FEP, the bending stiffness of PSU/FEP and PC/FEP fibers is several times smaller than that of CYTOP and PMMA fibers. For example, the bending stiffness of CYTOP and PMMA fibers is 11.8 N/m and 22 N/m, respectively when the length of the probes is set to 8 mm. By contrast, that of the PC/FEP and PSU FEP POFs are 4.96 N/m and 5.02 N/m, respectively using the same length. It is noteworthy that the bending stiffness difference between PC/FEP and PSU/FEP fibers is insignificant, which is why they are overlapped with each other in figure 4(a). Figures 4(b) and (c) illustrate the bending stiffness variation of PC/FEP and PS/FEP POFs as a function of fiber diameter and length. For comparison, the bending stiffness of two commercially available silica fibers is plotted in these figures as a dotted line. The silica fibers chosen in our investigations are widely used in fiber-based neural applications: FG105LCA (Diameter: 125 μm) and FT200EMT (Diameter: 225 μm) from Thorlabs, both evaluated assuming a length of 10 mm. The advantages in terms of the mechanical properties of the presented fibers with respect to the current standard in the field of neuroscience are underlined by these numerical results. Indeed, for their bending stiffness to reach values similar to the ones of the thin silica fibers (i.e. 125 μm), the UHNA POFs should have a diameter larger than 300 μm.

The functionality of the MFCs was firstly evaluated by using them to inject 2 μL of 0.4% trypan blue dye solution to the 0.6% agarose brain phantom with an injection rate of 100 nL/min as shown in figures 4(d) and (e). The dye flowed through the MFCs without leaking and was evenly diffused in the medium (figure 4 (e)). Figure 4 (f) shows that 10 μL trypan blue dye was injected by the MFCs with different target rates at 10, 50, 100, 500, and 1000 nL/min. For all measurements, the output rate was found to be equal to the injection rate, verifying the functionality of the integrated MFCs in our POFs to act as a precise tool for on-demand drug delivery.

Accepted Manuscript

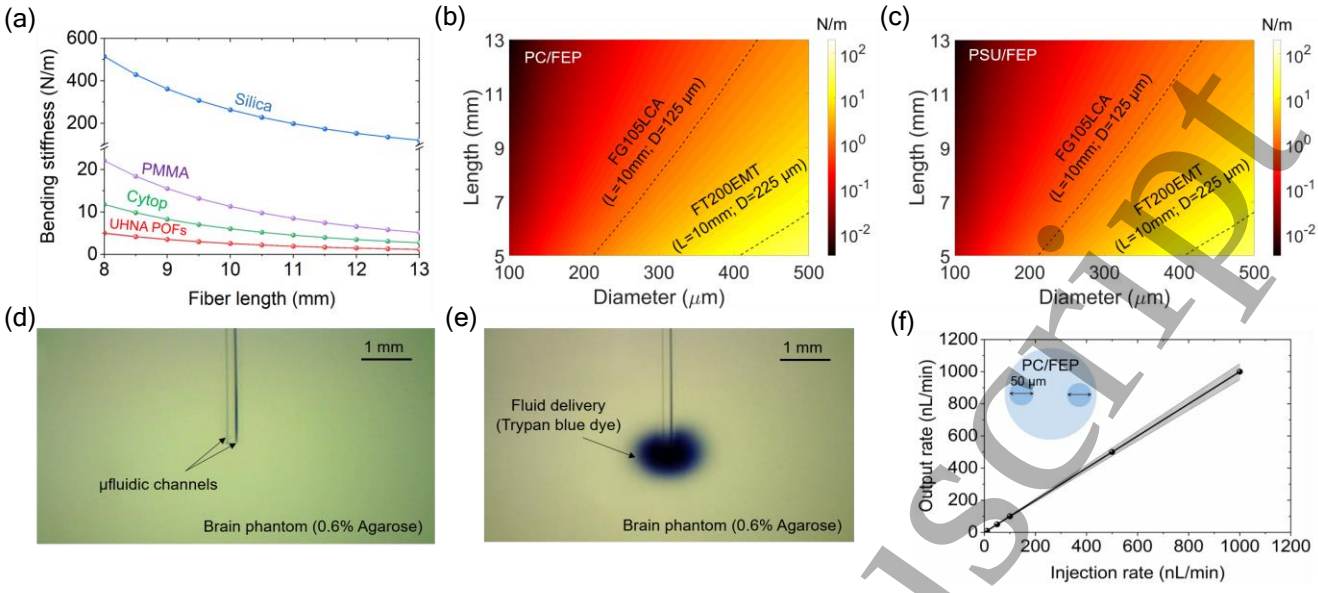


Figure 4. (a) Comparison of calculated bending stiffness between PSU/FEP, PC/FEP, silica, CYTOP, and PMMA fibers. (b),(c) Bending stiffness as a function of fiber diameter and length for PC/FEP and PSU/FEP respectively. (d),(e) PC/FEP fiber with trypan blue loaded inside the MFCs, before and after injection, respectively. (f) Output rate as a function of injection rate by the MFCs in 1 cm long PC/FEP fibers.

3.2 Illumination map in brain phantom

In figure 5, we show the illumination map in the brain phantom of the UHNA POFs compared to standard commercial silica fibers (NA=0.39). For these experiments, two different excitation wavelengths have been used, i.e. 470 nm and 650 nm. The direct comparison of the 2D illumination maps involving the PC/FEP and PSU/FEP POFs are shown in (figures 5(a),(b)) and (Figures 5(c),(d)), respectively. Iso-intensity contours in these images define the boundaries at which intensity falls to 5%, 10%, 25%, 50%, and 75% of its maximum are shown in white, green, yellow, orange, and red, respectively. In the bottom row of figure 5, the corresponding 3D iso-intensity surfaces defining the boundaries at which intensity falls to 5%, 10%, 25%, 50%, and 75% of its maximum for silica fibers and UHNA POFs are shown in black, blue, green, orange, and red, respectively. This is used to further highlight the difference in illumination volume between silica and UHNA POFs in 3D space. Table 2 summarizes the illumination area of the fibers in figure 5(a-d) with the unit of mm^2 to quantitatively indicate how the increased illumination angle from the UHNA POFs leads to a larger area. The illumination area as a percentage of the total area of the figure is also indicated in parentheses. One can see that the increased illuminated area of UHNA POFs is more evident when intensity falls to 5% of maximum compared to the relatively low NA silica optical fibers.

Accepted Manuscript

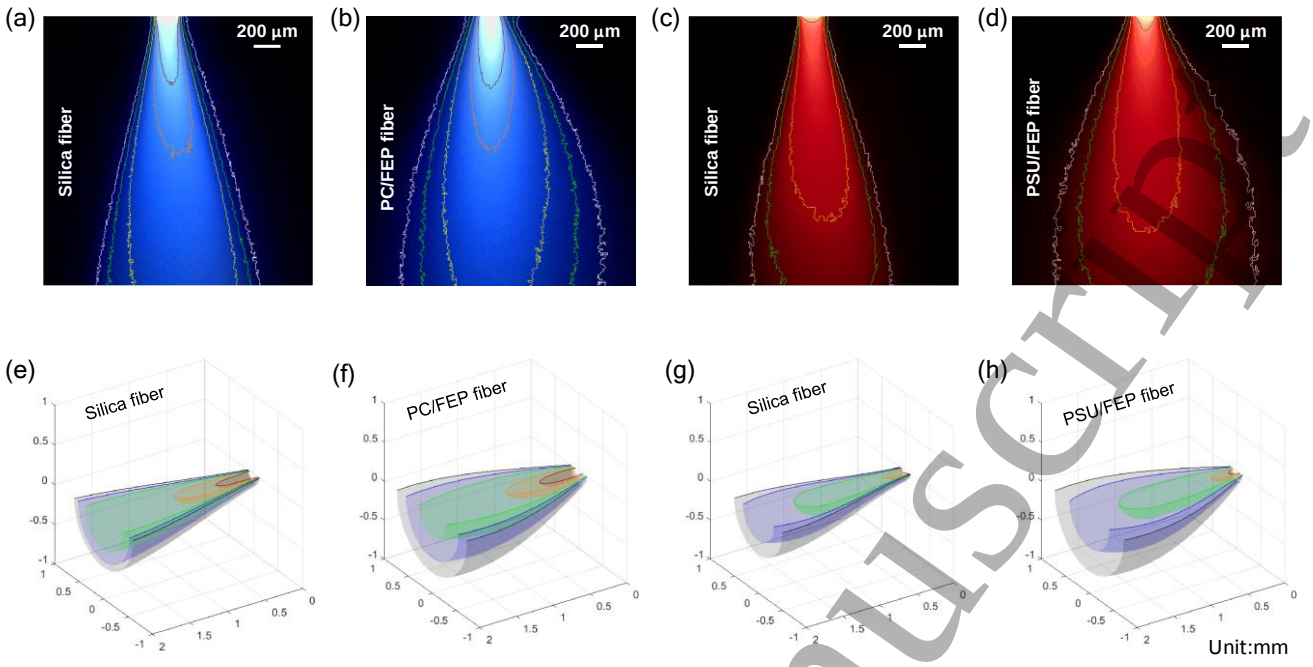


Figure 5. (a), (b) Experimentally measured illumination map at 470 nm in brain phantom (0.6% agarose gels) from a commercial silica fiber and the PC/FEP fiber, respectively. (c),(d) Illumination map measured with 650 nm in brain phantom from a commercial silica fiber and the PSU/FEP fiber, respectively. Iso-intensity contours are plotted in these images to highlight the boundaries at which the light intensity falls below 5% (white), 10% (green), 25% (yellow), 50% (orange), and 75% (red) of its maximum. (e) (f) (g) (h) Cross-sections of the 3-dimensional reconstruction of the illumination area for the corresponding measured profiles. Iso-intensity surfaces defining the boundaries at which intensity falls to 5%, 10%, 25%, 50%, and 75% of its maximum are shown in black, blue, green, orange, and red, respectively.

Table 2. Illumination Area (unit mm^2)

Light Source (wavelength)	**LED (470 nm)**		**LED (650 nm)**	
Fiber	Silica Fibers	PC/FEP POFs	Silica Fibers	PSU/FEP POFs
NA	0.39	0.87	0.39	0.84
>75%	0.064 (1.61%)	0.086 (2.14%)	0.005 (0.13%)	0.01 (0.25%)
>50%	0.223 (5.58%)	0.257 (6.41%)	0.032 (0.8%)	0.047(1.17%)
>25%	1.086 (27.16%)	1.257 (31.42%)	0.454 (11.34%)	0.613 (15.34%)
>10%	1.313 (32.82%)	1.783 (44.58%)	1.097 (27.43%)	1.611 (40.28%)
>5%	1.506 (37.65%)	2.187 (54.68%)	1.349 (33.73%)	2.172 (54.3%)

3.3 Illumination map in brain slice

In optogenetic experiments, tissue can not only be damaged by the mechanical mismatch between the implant and tissue but also by an excessive power density of the stimulating light [62]. The opsins should be activated by a power density that, while being higher than the excitation threshold, remains below the phototoxicity threshold. Dubois *et al.* [57] have performed numerical simulations to optimize the design of

Accepted Manuscript

optical fibers to achieve minimally invasive optogenetics stimulation or photomodulation of deep and large cortical areas with red light in the non-human primate brain. In these simulations, in which the diameter of the fiber is fixed to 500 µm, it is shown that when increasing the fiber's NA from 0.1 to 0.9, the penetration depth of the red light reduces and the lateral spread of the light becomes wider. Consequently, fibers with a large numerical aperture are preferable since they can effectively decrease the power density in the illuminated brain layer and reduce light-induced tissue damage. Because of the lack of optical fibers with NA higher than 0.5, the illumination map from UHNA optical fibers has only been numerically demonstrated so far. Here, for the first time, an experimental comparison between the illumination map of UHNA POFs and commercial silica fibers in real brain tissue is presented. To image the illumination map in brain tissue, the experimental setup (configuration 1) presented in figure 3 was used, by substituting the artificial phantom with a brain slice of 700 µm thickness. The central wavelength of the LED source was 650 nm and the power was set to 50 µW. Figure 6 shows the iso-intensity contours in the images defining the boundaries at which the intensity falls to 10%, 25%, 50%, 75%, and 90% of its maximum. By comparing the two images, one can see a significant light expansion in the lateral direction where the UHNA POFs are used. However, this effect is reducing as depth increases since the light is strongly diffused by the brain tissue. Our experimental result was found to be consistent with the simulation investigation from Dubois *et al.* [57]

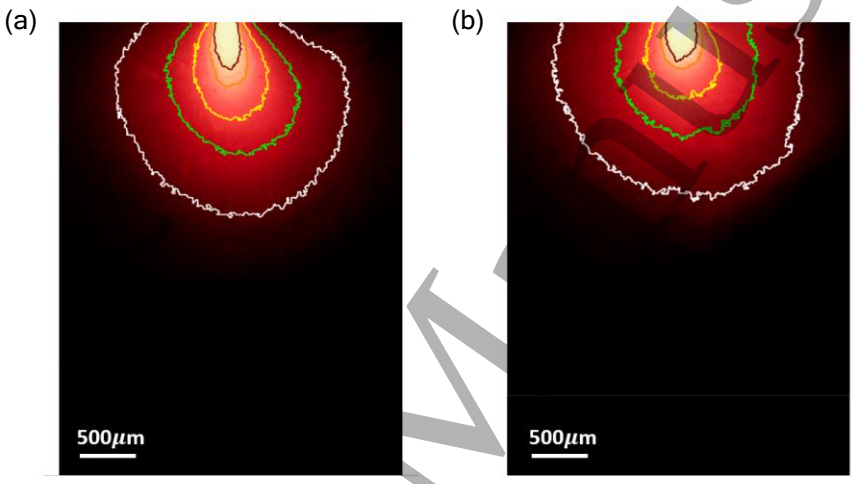


Figure 6. Illumination map at 650 nm wavelength measured in the brain slice using (a) commercial silica fiber (NA=0.39), and (b) UHNA POF (NA=0.84), respectively. Iso-intensity contours in the images defining the boundaries at which intensity falls to 10%, 25%, 50%, 75%, and 90% of its maximum are shown in white, green, yellow, orange, and red, respective

3.4 Fluorescent light recording

Optical fibers have also a crucial role in fiber photometry applications [63,64]. In order to verify the capability of our UHNA POFs to be used as an efficient optical waveguide in a fluorescent light recording system, the position of the fibers was scanned using a custom-made motorized system from -500 µm to 500 µm in both X and Y direction with a step of 50 µm after the center of the fiber end-facet has been aligned to the fluorescent PS bead (figure 7(a) and (b)). The backward fluorescent light intensity was detected using a sensitive photodetector and recorded by the DAQ for each X-Y position. The normalized 2D detected fluorescent light intensity is shown in figure 7(c). Although the excitation light and backward fluorescent light have been strongly scattered by the brain tissue, one can see that the position of the fluorescent PS bead was identified in the center of the map clearly, which is consistent with the physical position of the PS bead. This suggests that the photometry system based on UHNA POFs can act as an accurate fluorescent light recording in each position of the scanning process. Our results indicate that the developed UHNA POFs can be employed for fluorescent light recording in fiber photometry setup. In addition, the UHNA POFs have the potential to be fabricated as fiber bundles for *in vivo* fluorescent light imaging in the deep brain without requiring the scanning process [25].

Accepted Manuscript

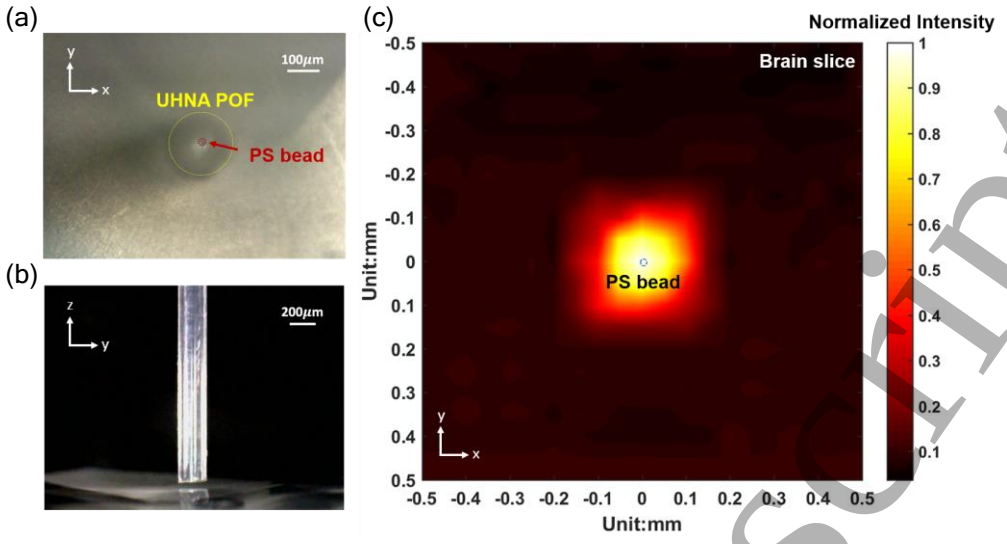


Figure 7. The end-facet of the optical fiber is aligned to the PS bead in both (a) X-Y and (b) Z direction, acquired by the digital microscope (see figure 3(b) and (c), respectively). (c) The collected map of the fluorescent light of a bead by UHNA based fiber photometry. The position of the fiber scans from -0.5 mm to +0.5 mm away from the original place in both X and Y directio

4. Discussion

This work demonstrates for the first time the development of UHNA fiber neural devices based on soft polymer materials for enlarging the output illumination angle towards efficient neuromodulation of brain activity. The highest commercially available silica optical fibers have an NA of 0.5, a fact that can result in a limitation to the applications of optogenetics in the deep brain region. Although some researchers have developed UHNA microstructured silica fibers by introducing a photonic crystal cladding [32,65] (NA as high as 0.61), such fibers are not suitable for being implanted in the brain since the biological liquids from the tissue could enter the hollow channels and detrimentally change the light propagation properties [66]. Recently, silica fibers with a tapered structure have been reported that can act as an alternative route for increasing illumination area in neural tissues [67,68]. However, such structures are based on stiff and fragile glass materials and would therefore inevitably cause the same inflammation issues as conventional silica optical fibers. Polymers are thus a promising candidate as the host material for the fabrication of optical fiber-based implants. Even though several step-index POFs have already been developed for this application, POFs with NA higher than 0.5 do not exist, to the best of our knowledge. Therefore, here we propose two new UHNA POFs enabled by using a very soft material (FEP) for the first time. The low RI of this material creates new possibilities to significantly increase the NA of step-index POFs. Furthermore, the high softness (low Young's modulus) of FEP endows this material with a natural advantage to reduce the FBR and thus provide the possibility to conduct improved chronic experiments involving optical neuromodulation and fiber photometry. The presented fiber devices can be also developed to advanced multifunctional neural interfaces. Here, we demonstrated the possibility of integrating MFCs in the FEP cladding, however more functional structures can be added in the cross-section of the fiber such as metal electrodes for electrophysiology application [21,22,69].

In this work, we investigate the illumination performance of the developed fibers as implants in phantom and brain slices. It is worth noticing that scattering and absorption characteristics can vary widely between different tissues, resulting in a strong difference in terms of the illuminated area. For example, Al-Juboori *et al.* have found that the effective scattering coefficient of the Ventral Nucleus of the Trapezoid Body (VNTB) of C57BL/6J mice is 199.6 cm^{-1} at 453 nm wavelength while that of the cerebellum is only 97.6 cm^{-1} at the same wavelength [70]. Since the scattering coefficient can dramatically vary across different brain regions, here we focused on comparing the illumination map of the brain phantom (0.6% agarose) and the prefrontal cortex of adult rats. The reason we selected brain phantom and real brain slices is because the former (i.e. brain phantom made by 0.6% agarose gels) has been extensively used as a reliable testbed for *in vitro* studies of neurological modalities involving light-brain interaction [43]. The latter (i.e. adult rat cortex) on the other hand is one of the most commonly used

Accepted Manuscript

parts of the brain for optogenetics [7,71]. Our results indicate that when we use the brain phantom, the illumination area of the UHNA fiber is significantly increased compared to the standard commercial silica fibers. When we replace the brain phantom with real brain tissue, the strong scattering introduced by the sample limits the illuminated area, while allows lateral expansion of the light distribution and consequently leads to a lower power density at the various brain layers, reducing the light-induced thermal damage [57].

5. Conclusion

In summary, two different optical fibers based on two sets of polymers are presented: PC/FEP and PSU/FEP. Two MFCs have been added to the cladding of the PC/FEP POFs for accurate on-demand drug delivery. The numerical analysis based on the finite element method shows that the bending stiffness of these POFs is 100 times lower than that of commercial silica fibers, a property that is critical in brain implants that are to be used in neuroscience. The performance of the developed fiber devices was characterized in both brain phantom and real slice. Compared with commercial silica optical fibers, the illumination area (defined as the region of the sample reached by at least 5% of the maximum light intensity) is enlarged by 17% and 21% at 470 nm and 650 nm wavelength, respectively. When illuminating a brain slice, the expanded lateral distribution of the light from the output of the UHNA-POFs with respect to silica optical fiber was demonstrated, showing the potential for reducing light power density and subsequently avoiding light (thermal)-induced tissue damage [57]. Furthermore, the fabricated POFs were used for fluorescent light recording demonstrating their ability to be used for fiber photometry. In conclusion, we believe that the presented fiber devices constitute an efficient route for the development of fiber-based neural probes based on advanced optical materials towards biocompatible multifunctional tools for long-term optical neuromodulation in freely behaving animals as well as high-resolution fluorescence imaging.

Acknowledgments

The authors acknowledge support from the Multi-BRAIN project funded by the Lundbeck Foundation (R276-2018-869).

References

[1] Chen R, Canales A and Anikeeva P 2017 Neural Recording and Modulation Technologies *Nat Rev Mater* **2** 16093

[2] Luan S, Williams I, Nikolic K and Constandinou T G 2014 Neuromodulation: present and emerging methods *Front Neuroeng* **7** 27

[3] Häusser M 2014 Optogenetics: the age of light *Nature Methods* **11** 1012–4

[4] Kalanithi P S A and Henderson J M 2012 Optogenetic neuromodulation *Int Rev Neurobiol* **107** 185–205

[5] Tyler W J, Sanguinetti J L, Fini M and Hool N 2017 Non-invasive neural stimulation *Micro- and Nanotechnology Sensors, Systems, and Applications IX* Micro- and Nanotechnology Sensors, Systems, and Applications IX vol 10194 (International Society for Optics and Photonics) p 101941L

[6] Bao G, Mitragotri S and Tong S 2013 Multifunctional Nanoparticles for Drug Delivery and Molecular Imaging *Annual Review of Biomedical Engineering* **15** 253–82

[7] Aravanis A M, Wang L-P, Zhang F, Meltzer L A, Mogri M Z, Schneider M B and Deisseroth K 2007 An optical neural interface:in vivocontrol of rodent motor cortex with integrated fiberoptic and optogenetic technology *J. Neural Eng.* **4** S143–56

[8] Nazempour R, Zhang Q, Fu R and Sheng X 2018 Biocompatible and Implantable Optical Fibers and Waveguides for Biomedicine *Materials* **11** 1283

[9] Sparta D R, Stamatakis A M, Phillips J L, Hovelsø N, van Zessen R and Stuber G D 2012 Construction of implantable optical fibers for long-term optogenetic manipulation of neural circuits *Nature Protocols* **7** 12–23

[10] Spearman B S, Desai V H, Mobini S, McDermott M D, Graham J B, Otto K J, Judy J W and Schmidt C E 2018 Tissue-Engineered Peripheral Nerve Interfaces *Advanced Functional Materials* **28** 1701713

[11] Skutnik B J 2010 High-NA HPCS optical fibers for medical diagnosis and treatment *Optical Fibers and Sensors for Medical Diagnostics and Treatment Applications X* Optical Fibers and Sensors for Medical Diagnostics and Treatment Applications X vol 7559 (International Society for Optics and Photonics) p 75590M

[12] Bianchi S, Rajamanickam V P, Ferrara L, Fabrizio E D, Liberale C and Leonardo R D 2013 Focusing and imaging with increased numerical apertures through multimode fibers with micro-fabricated optics *Opt. Lett., OL* **38** 4935–8

[13] Harmon J P 2001 Polymers for Optical Fibers and Waveguides: An Overview *Optical Polymers* ACS Symposium Series vol 795 (American Chemical Society) pp 1–23

Accepted Manuscript

[14] Fasano A, Woyessa G, Stajanca P, Markos C, Stefani A, Nielsen K, Rasmussen H K, Krebber K and Bang O 2016 Fabrication and characterization of polycarbonate microstructured polymer optical fibers for high-temperature-resistant fiber Bragg grating strain sensors *Opt. Mater. Express, OME* **6** 649–59

[15] Peters K 2010 Polymer optical fiber sensors—a review *Smart Mater. Struct.* **20** 013002

[16] Markos C, Yuan W, Vlachos K, Town G E and Bang O 2011 Label-free biosensing with high sensitivity in dual-core microstructured polymer optical fibers *Opt. Express, OE* **19** 7790–8

[17] Fan B, Kwon K Y, Weber A J and Li W 2014 An implantable, miniaturized SU-8 optical probe for optogenetics-based deep brain stimulation *2014 36th Annual International Conference of the IEEE Engineering in Medicine and Biology Society* 2014 36th Annual International Conference of the IEEE Engineering in Medicine and Biology Society pp 450–3

[18] Choi M, Choi J W, Kim S, Nizamoglu S, Hahn S K and Yun S H 2013 Light-guiding hydrogels for cell-based sensing and optogenetic synthesis in vivo *Nature Photonics* **7** 987–94

[19] Fu R, Luo W, Nazempour R, Tan D, Ding H, Zhang K, Yin L, Guan J and Sheng X 2018 Implantable and Biodegradable Poly(l-lactic acid) Fibers for Optical Neural Interfaces *Advanced Optical Materials* **6** 1700941

[20] Lu C, Froriep U P, Koppes R A, Canales A, Caggiano V, Selvidge J, Bizzi E and Anikeeva P 2014 Polymer Fiber Probes Enable Optical Control of Spinal Cord and Muscle Function In Vivo *Advanced Functional Materials* **24** 6594–600

[21] Canales A, Jia X, Froriep U P, Koppes R A, Tringides C M, Selvidge J, Lu C, Hou C, Wei L, Fink Y and Anikeeva P 2015 Multifunctional fibers for simultaneous optical, electrical and chemical interrogation of neural circuits in vivo *Nature Biotechnology* **33** 277–84

[22] Frank J A, Antonini M-J, Chiang P-H, Canales A, Konrad D B, Garwood I C, Rajic G, Koehler F, Fink Y and Anikeeva P 2020 In Vivo Photopharmacology Enabled by Multifunctional Fibers *ACS Chem. Neurosci.* **11** 3802–13

[23] Park S, Guo Y, Jia X, Choe H K, Grena B, Kang J, Park J, Lu C, Canales A, Chen R, Yim Y S, Choi G B, Fink Y and Anikeeva P 2017 One-step optogenetics with multifunctional flexible polymer fibers *Nature Neuroscience* **20** 612–9

[24] Shan D, Zhang C, Kalaba S, Mehta N, Kim G B, Liu Z and Yang J 2017 Flexible biodegradable citrate-based polymeric step-index optical fiber *Biomaterials* **143** 142–8

[25] Guo Y, Werner C F, Canales A, Yu L, Jia X, Anikeeva P and Yoshinobu T 2020 Polymer-fiber-coupled field-effect sensors for label-free deep brain recordings *PLOS ONE* **15** e0228076

[26] Patiño-Jurado B, Botero-Cadavid J F and Garcia-Sucerquia J 2019 Analytical study of the numerical aperture of cone-shaped optical fibers: A tool for tailored designs *Heliyon* **5** e01612

[27] Woyessa G, Fasano A, Markos C, Rasmussen H K and Bang O 2017 Low Loss Polycarbonate Polymer Optical Fiber for High Temperature FBG Humidity Sensing *IEEE Photonics Technology Letters* **29** 575–8

[28] Greer A I M, Vasiev I, Della-Rosa B and Gadegaard N 2016 Fluorinated ethylene–propylene: a complementary alternative to PDMS for nanoimprint stamps *Nanotechnology* **27** 155301

[29] Park S 2018 *Multifunctional fiber-based neural interfaces* Thesis (Massachusetts Institute of Technology)

[30] Park S, Yuk H, Zhao R, Yim Y S, Woldeghebriel E W, Kang J, Canales A, Fink Y, Choi G B, Zhao X and Anikeeva P 2021 Adaptive and multifunctional hydrogel hybrid probes for long-term sensing and modulation of neural activity *Nat Commun* **12** 3435

[31] Keathley P D and Hastings J T 2008 Optical properties of sputtered fluorinated ethylene propylene and its application to surface-plasmon resonance sensor fabrication *Journal of Vacuum Science & Technology B: Microelectronics and Nanometer Structures Processing, Measurement, and Phenomena* **26** 2473–7

[32] Wadsworth W J, Percival R M, Bouwmans G, Knight J C, Birks T A, Hedley T D and Russell P S J 2004 Very high numerical aperture fibers *IEEE Photonics Technology Letters* **16** 843–5

[33] Akrami P, Adamu A I, Woyessa G, Rasmussen H K, Rasmussen H K, Bang O and Markos C 2021 All-polymer multimaterial optical fiber fabrication for high temperature applications *Opt. Mater. Express, OME* **11** 345–54

Accepted Manuscript

[34] Chen M, Wang Z, Zhang Q, Wang Z, Liu W, Chen M and Wei L 2021 Self-powered multifunctional sensing based on super-elastic fibers by soluble-core thermal drawing *Nature Communications* **12** 1416

[35] Tao G, Ebendorff-Heidepriem H, Stolyarov A M, Danto S, Badding J V, Fink Y, Ballato J and Abouraddy A F 2015 Infrared fibers *Adv. Opt. Photon., AOP* **7** 379–458

[36] Park S, Loke G, Fink Y and Anikeeva P 2019 Flexible fiber-based optoelectronics for neural interfaces *Chemical Society Reviews* **48** 1826–52

[37] Xie C, Liu J, Fu T-M, Dai X, Zhou W and Lieber C M 2015 Three-dimensional macroporous nanoelectronic networks as minimally invasive brain probes *Nature Materials* **14** 1286–92

[38] Dai Y, Xue Y and Zhang J 2015 Vibration-Based Milling Condition Monitoring in Robot-Assisted Spine Surgery *IEEE/ASME Transactions on Mechatronics* **20** 3028–39

[39] Rangel Guerrero D K, Donnett J G, Csicsvari J and Kovács K A 2018 Tetrode Recording from the Hippocampus of Behaving Mice Coupled with Four-Point-Irradiation Closed-Loop Optogenetics: A Technique to Study the Contribution of Hippocampal SWR Events to Learning *eNeuro* **5**

[40] Thomas K A and Cook S D 1985 An evaluation of variables influencing implant fixation by direct bone apposition *Journal of Biomedical Materials Research* **19** 875–901

[41] Dooher T, McGarrigle C, Dixon D, Mcilhagger A, Harkin-Jones FREng E and Archer E 2017 Novel thermoplastic yarn for the through-thickness reinforcement of fibre-reinforced polymer composites *Journal of Thermoplastic Composite Materials* **31** 089270571774329

[42] Chapalo I, Theodosiou A, Kalli K and Kotov O 2020 Multimode Fiber Interferometer Based on Graded-Index Polymer CYTOP Fiber *Journal of Lightwave Technology* **38** 1439–45

[43] Allison S W and Gillies G T 2010 Fluorescence excitation and propagation through brain phantom gelatins: measurements and potential applications *Meas. Sci. Technol.* **21** 085802

[44] El Waly B, Escarrat V, Perez-Sanchez J, Kaur J, Pelletier F, Collazos-Castro J E and Debarbieux F 2021 Intravital Assessment of Cells Responses to Conducting Polymer-Coated Carbon Microfibres for Bridging Spinal Cord Injury *Cells* **10** 73

[45] Kaur J, Mazzone G L, Aquino J B and Nistri A 2021 Nicotine Neurotoxicity Involves Low Wnt1 Signaling in Spinal Locomotor Networks of the Postnatal Rodent Spinal Cord *International Journal of Molecular Sciences* **22** 9572

[46] Kaur J, Flores Gutiérrez J and Nistri A 2016 Neuroprotective effect of propofol against excitotoxic injury to locomotor networks of the rat spinal cord in vitro *European Journal of Neuroscience* **44** 2418–30

[47] Kaur J, Rauti R and Nistri A 2018 Nicotine-mediated neuroprotection of rat spinal networks against excitotoxicity *European Journal of Neuroscience* **47** 1353–74

[48] Lin J Y, Lin M Z, Steinbach P and Tsien R Y 2009 Characterization of Engineered Channelrhodopsin Variants with Improved Properties and Kinetics *Biophysical Journal* **96** 1803–14

[49] Yizhar O, Fenno L E, Prigge M, Schneider F, Davidson T J, O'Shea D J, Sohal V S, Goshen I, Finkelstein J, Paz J T, Stehfest K, Fudim R, Ramakrishnan C, Huguenard J R, Hegemann P and Deisseroth K 2011 Neocortical excitation/inhibition balance in information processing and social dysfunction *Nature* **477** 171–8

[50] Lin J Y, Knutsen P M, Muller A, Kleinfeld D and Tsien R Y 2013 ReaChR: a red-shifted variant of channelrhodopsin enables deep transcranial optogenetic excitation *Nature Neuroscience* **16** 1499–508

[51] Oda K, Vierock J, Oishi S, Rodriguez-Rozada S, Taniguchi R, Yamashita K, Wiegert J S, Nishizawa T, Hegemann P and Nureki O 2018 Crystal structure of the red light-activated channelrhodopsin Chrimson *Nature Communications* **9** 3949

[52] Zhang F, Prigge M, Beyrière F, Tsunoda S P, Mattis J, Yizhar O, Hegemann P and Deisseroth K 2008 Red-shifted optogenetic excitation: a tool for fast neural control derived from Volvox carteri *Nature Neuroscience* **11** 631–3

[53] Armstrong C, Krook-Magnuson E, Oijala M and Soltesz I 2013 Closed-loop optogenetic intervention in mice *Nature Protocols* **8** 1475–93

[54] Chen C H, McCullagh E A, Pun S H, Mak P U, Vai M I, Mak P I, Klug A and Lei T C 2017 An Integrated Circuit for Simultaneous Extracellular Electrophysiology Recording and Optogenetic Neural

Accepted Manuscript

Manipulation *IEEE Transactions on Biomedical Engineering* **64** 557–68

[55] Pelluru D, Konadhode R R, Bhat N R and Shiromani P J 2016 Optogenetic stimulation of astrocytes in the posterior hypothalamus increases sleep at night in C57BL/6J mice *European Journal of Neuroscience* **43** 1298–306

[56] Yona G, Meitav N, Kahn I and Shoham S 2016 Realistic Numerical and Analytical Modeling of Light Scattering in Brain Tissue for Optogenetic Applications *eNeuro* **3**

[57] Dubois A, Chiang C-C, Smekens F, Jan S, Cuplov V, Palfi S, Chuang K-S, Senova S and Pain F 2018 Optical and thermal simulations for the design of optodes for minimally invasive optogenetics stimulation or photomodulation of deep and large cortical areas in non-human primate brain *J. Neural Eng.* **15** 065004

[58] Muir J, Lorsch Z S, Ramakrishnan C, Deisseroth K, Nestler E J, Calipari E S and Bagot R C 2018 In Vivo Fiber Photometry Reveals Signature of Future Stress Susceptibility in Nucleus Accumbens *Neuropsychopharmacol.* **43** 255–63

[59] Mansy M M, Kim H and Oweiss K G 2019 Spatial detection characteristics of a single photon fiber photometry system for imaging neural ensembles* *2019 9th International IEEE/EMBS Conference on Neural Engineering (NER)* 2019 9th International IEEE/EMBS Conference on Neural Engineering (NER) pp 969–72

[60] Perkins L N, Semu D, Shen J, Boas D A and Gardner T J 2018 High-density microfibers as a potential optical interface to reach deep brain regions *J. Neural Eng.* **15** 066002

[61] Du M, Huang L, Zheng J, Xi Y, Dai Y, Zhang W, Yan W, Tao G, Qiu J, So K-F, Ren C and Zhou S 2020 Flexible Fiber Probe for Efficient Neural Stimulation and Detection *Advanced Science* **7** 2001410

[62] Galvan A, Stauffer W R, Acker L, El-Shamayleh Y, Inoue K, Ohayon S and Schmid M C 2017 Nonhuman Primate Optogenetics: Recent Advances and Future Directions *J. Neurosci.* **37** 10894–903

[63] Pisanello M, Pisano F, Hyun M, Maglie E, Balena A, De Vittorio M, Sabatini B L and Pisanello F 2019 The Three-Dimensional Signal Collection Field for Fiber Photometry in Brain Tissue *Frontiers in Neuroscience* **13** 82

[64] Pisano F, Pisanello M, Lee S J, Lee J, Maglie E, Balena A, Sileo L, Spagnolo B, Bianco M, Hyun M, De Vittorio M, Sabatini B L and Pisanello F 2019 Depth-resolved fiber photometry with a single tapered optical fiber implant *Nat Methods* **16** 1185–92

[65] Amitonova L V, Descloux A, Petschulat J, Frosz M H, Ahmed G, Babic F, Jiang X, Mosk A P, Russell P S J and Pinkse P W H 2016 High-resolution wavefront shaping with a photonic crystal fiber for multimode fiber imaging *Opt. Lett., OL* **41** 497–500

[66] Markos C, Travers J C, Abdolvand A, Eggleton B J and Bang O 2017 Hybrid photonic-crystal fiber *Rev. Mod. Phys.* **89** 045003

[67] Pisanello M, Pisano F, Sileo L, Maglie E, Bellistri E, Spagnolo B, Mandelbaum G, Sabatini B L, De Vittorio M and Pisanello F 2018 Tailoring light delivery for optogenetics by modal demultiplexing in tapered optical fibers *Sci Rep* **8** 4467

[68] Pisanello F, Mandelbaum G, Pisanello M, Oldenburg I A, Sileo L, Markowitz J E, Peterson R E, Della Patria A, Haynes T M, Emara M S, Spagnolo B, Datta S R, De Vittorio M and Sabatini B L 2017 Dynamic illumination of spatially restricted or large brain volumes via a single tapered optical fiber *Nat Neurosci* **20** 1180–8

[69] Jiang S, Patel D C, Kim J, Yang S, Mills W A, Zhang Y, Wang K, Feng Z, Vijayan S, Cai W, Wang A, Guo Y, Kimbrough I F, Sontheimer H and Jia X 2020 Spatially expandable fiber-based probes as a multifunctional deep brain interface *Nat Commun* **11** 6115

[70] Al-Juboori S I, Dondzillo A, Stubblefield E A, Felsen G, Lei T C and Klug A 2013 Light Scattering Properties Vary across Different Regions of the Adult Mouse Brain *PLOS ONE* **8** e67626

[71] Liang Z, Watson G D R, Alloway K D, Lee G, Neuberger T and Zhang N 2015 Mapping the functional network of medial prefrontal cortex by combining optogenetics and fMRI in awake rats *NeuroImage* **117** 114–23

Accepted Manuscript